

Task-Aware Active Learning for Endoscopic Image Analysis

Shrawan Kumar Thapa², Pranav Poudel³, Binod Bhattarai^{1*}, and Danail Stoyanov¹

¹ University College London, UK

² NAAMII, Nepal

³ IOE Pulchowk Campus, Nepal

{b.bhattarai,danail.stoyanov}@ucl.ac.uk

Abstract. Semantic segmentation of polyps and depth estimation are two important research problems in endoscopic image analysis. One of the main obstacles to conduct research on these research problems is lack of annotated data. Endoscopic annotations necessitate the specialist knowledge of expert endoscopists and due to this, it can be difficult to organise, expensive and time consuming. To address this problem, we investigate an active learning paradigm to reduce the number of training examples by selecting the most discriminative and diverse unlabelled examples for the task taken into consideration. Most of the existing active learning pipelines are task-agnostic in nature and are often sub-optimal to the end task. In this paper, we propose a novel task-aware active learning pipeline and applied for two important tasks in endoscopic image analysis: semantic segmentation and depth estimation. We compared our method with the competitive baselines. From the experimental results, we observe a substantial improvement over the compared baselines. Codes are available at <https://github.com/thetna/endo-active-learn>.

Keywords: Active Learning · Surgical AI · Endoscopic Image Analysis · Computer Assisted Interventions · Depth Estimation · Semantic Segmentation

1 Introduction

Polyp segmentation [3,2] and depth estimation [12] are two fundamental research problems in endoscopic image analysis. Automatic polyp segmentation can help in the early diagnosis, detection and treatment of colorectal disease by supporting endoscopists with computer assisted detection and characterization systems. Meanwhile depth estimation is essential for 3D surface reconstruction of the endoluminal environment and for creating systems to map the colon shape and ensure that the full organ and all tissue surfaces are appropriately examined. Both capabilities are needed to advance the toolkit available to endoscopists

* Corresponding author

and enable standardization of adenoma detection rates and potentially link to future robotic systems and automation [1].

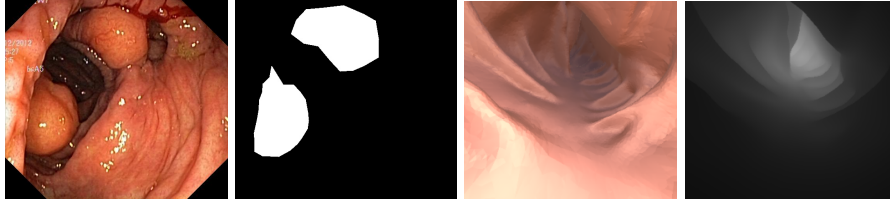


Fig. 1. Two left most images are from Kvasir-SEG [7], and the two right most images are from Colonoscopy Depth [12] data set.

The efficacy of the deep networks to learn the parameters for both tasks, polyp segmentation and depth estimation, has been demonstrated, however, most solutions demand a large number of training examples. Annotating such a large volumes of endoscopic data is expensive, needs experts, and it is time-consuming, and for certain tasks like depth estimation, the ground truth is inherently not available. Figure 1 shows a pair of randomly selected images from Kvasir-SEG [7] and Colonoscopy Depth [12] data sets. These are two important benchmarks publicly available for polyp segmentation and the depth estimation in endoscopy respectively.

Active Learning (AL) [13,15,5] has shown a lot of promises to become a viable solution to sub-sample the data set by discarding redundant and less informative examples in computer vision. Nowadays, it is also slowly getting popular in Biomedical Image Analysis [4,9]. NVIDIA’s open source platform MONAI ⁴ has launched an intelligent interactive data annotation tool called MONAI Label. Workshop with the theme ”interpretable and label-efficient learning” [6] was organised in conjunction with MICCAI 2020. There are few works already published in premier venues in medical image analysis. For example, Yang et. al. [17] proposed an AL framework for gland and lymph node segmentation based on class conditional uncertainty as a criterion to select unlabelled data. Similarly, [11] uses a conditional generative adversarial network to generate synthetic examples and estimate the uncertainties to select data to query their labels. Relying only on uncertainty as a selecting criterion helps us to choose the examples from the region of the manifolds of the image where the model is less confident. However, it can not avoid selecting the redundant images from the same manifold region, limiting the diversity. To address this issue, recently, Shi et al. [14] designed an AL framework for skin lesion detection aiming to select both the difficult and the diverse examples. To this end, the paper proposed to do hashing on the image features computed in an unsupervised manner by applying Principal Component Analysis (PCA) [16] and cluster the images into different bins.

⁴ <https://monai.io>

Next, the paper proposed to sample the images from each bin uniformly. This method addresses the issue of diversity that previous methods had. Nevertheless, the features computed in an unsupervised manner are not aware of the end task. Hence, the diverse examples on such sub-optimal features for the end task may not necessarily be diverse for the downstream task. As a result, the performance of the end task can be compromised.

To fulfil the criteria of task awareness and diversity in the selection mechanism, we proposed a novel framework for AL as shown in Figure 2. There are three main components in our pipeline: a Learner (A), a Sampler (B), and an oracle (C). The learner is responsible for learning the parameters for a downstream task by using the examples selected by the sampler. The oracle’s job is to query the labels of the examples selected by the learner. As the data selected by the sampler directly influences the learner’s performance, we argue the need for linkage between these two components. Therefore, we propose to project all the examples from a data set on the learner’s feature space before applying the sampler. Afterwards, we apply K-Center Greedy Algorithm similar to that in [13] to select the core-set of the unlabelled data set. The number of unlabelled examples we select in any selection-stage depend upon the budget. The examples chosen by the samplers are sent to oracle to query the labels and repeat the cycle.

We summarise our contributions in the following points.

- We proposed a task aware active learning algorithm to select representative and diverse examples to annotate their labels.
- We applied our method on two vital problems on endoscopic image analysis: polyp segmentation and depth estimation.
- We combined our method with uncertainty based AL method and observe improvement in the performance.

2 Method

Active Learning is an iterative process to select a subset of examples (\mathbf{X}^s) from a large pool of unlabelled set (\mathbf{X}) to query their labels (\mathbf{Y}). We label the examples $(\mathbf{x}, \mathbf{y}) \subset (\mathbf{X} \times \mathbf{Y})$ incrementally and add to a set of the labelled examples (\mathbf{X}^l). The labelled examples are used to train a network minimising the objective of the end task (\mathcal{L}). Equation 1 summarises the Active Learning pipeline. Given any sampling function \mathcal{A} , the main goal of AL is to minimise the number of selection stages n to reduce the number of examples to query their labels. In this paper, we have considered two important tasks: semantic segmentation and depth estimation in endoscopic image analysis.

$$\min_n \min_{\mathcal{L}} \mathcal{A}(\mathcal{L}(\mathbf{x}, \mathbf{y}; \theta) | \mathbf{X}_0^s \subset \dots \subset \mathbf{X}_n^s \subset \mathbf{X}). \quad (1)$$

To begin with annotation, we select the first batch \mathbf{X}_0^s randomly, where subscript 0 denotes the first selection stage and superscript s indicates a selected set of examples to query their labels. Once oracle queries their labels, we add those examples to the pool of labelled examples $\mathbf{X}^l = \{\mathbf{X}_0^s \cup \emptyset\}$. These labelled

examples act as seed annotations to guide the next selection stages. Figure 2 depicts the proposed method. There are three major components in the pipeline A) Learner, B) Sampler, and C) Oracle. We discuss these in detail below.

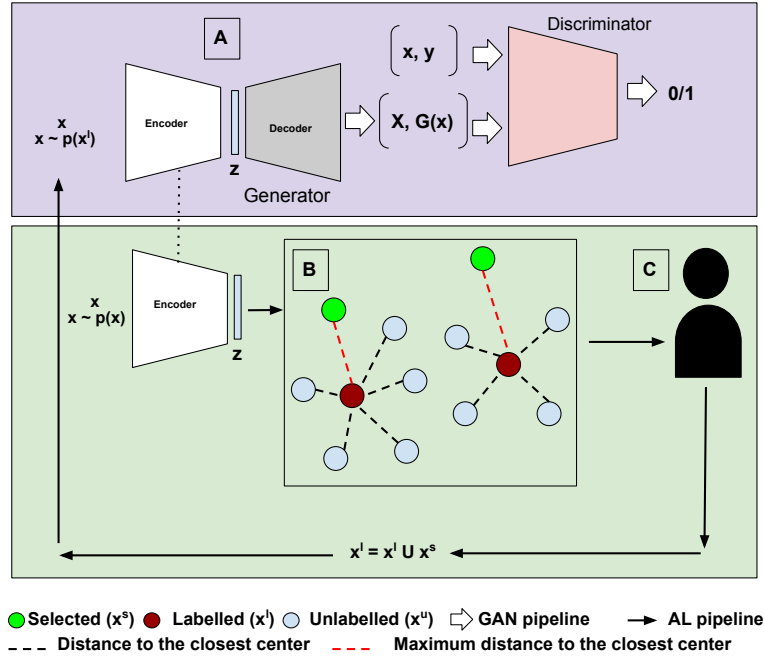


Fig. 2. Schematic diagram of the proposed Active Learning Pipeline.

Learner (A): The role of a learner in the AL is to learn the parameters for a downstream task from the labelled set of examples. In our case, we are tackling polyp segmentation and depth estimation, which are two key research problems in endoscopic image analysis. We choose pix2pix [18] to implement the learner. This architecture is well explored for semantic segmentation and depth estimation. For example, Rau et al. [12] obtained state-of-the-art performance on Colonoscopy Depth data set. Similar architectures are widely being used to tackle the semantic segmentation problems [3]. The learner consists of a generator (\mathbf{G}) and a discriminator (\mathbf{D}). Generator is an encoder-decoder architecture while discriminator is a CNN network with convolutional layers. Suppose, \mathbf{x} represents an image with its corresponding ground-truth label \mathbf{y} from labelled set \mathbf{X}^l . Depending on the problem taken into consideration, either semantic segmentation or depth map estimation, \mathbf{y} will be a ground truth semantic mask or a depth map. When we feed in \mathbf{x} on the generator, the encoder projects the image into a low dimensional vector, \mathbf{z} . And, the decoder reconstructs \mathbf{z} back to the

output $\mathbf{G}(\mathbf{x})$. We make a positive pair of (\mathbf{x}, \mathbf{y}) and $(\mathbf{x}, \mathbf{G}(\mathbf{x}))$ makes a negative pair. We feed these pairs to the discriminator to minimise the objective given in Equation 2. Both the generator and the discriminator learn the parameters competing with each other. Once we learn the parameters of GAN from the available labelled examples, we move to component B of the pipeline, which is a sampler.

$$\mathcal{L}(\mathbf{G}, \mathbf{D}) = \mathbb{E}_{(\mathbf{x}, \mathbf{y})}[\log(\mathbf{D}(\mathbf{x}, \mathbf{y}))] + \mathbb{E}_{(\mathbf{x}, \mathbf{G}(\mathbf{x}))}[\log(1 - \mathbf{D}(\mathbf{x}, \mathbf{G}(\mathbf{x})))] \quad (2)$$

Sampler (B): In this stage, we use the parameters of the encoder learned in stage A to project both the labelled examples and unlabelled images into a latent space, \mathbf{Z} . Since we train the learner to minimize the objective of the downstream task, the latent representations of the images are optimal for the downstream task. In Figure 2 block B, each node represents an image and node’s feature is initialised with the latent features extracted from the learner’s encoder. We propose to select a core set [13] of the data set based on this latent space in order to query their labels. To compute the core-set, we employ K-Center-Greedy algorithm on this latent space as shown in Algorithm 1. Referring to the Figure 2 block B, sky-blue nodes are unlabelled examples, red nodes are the labelled examples, and the green nodes are the selected examples to query their labels in the current stage. Please note, green nodes were sky-blue before selection. To select these green nodes, we compute the euclidean distance between the labelled examples with every unlabelled examples. The edges between the nodes represent the euclidean distances. The length is proportional to the magnitude of the distances. Higher the euclidean distance, longer is the edge. We create a territory of the nearest examples for each red nodes and select the farthest node amongst these ones as shown in the Figure. Examples with least euclidean distances are likely to be duplicates to the selected examples and does not provide a significant extra information to the downstream task. Hence, this selection strategy helps us to obtain a subset of representative examples of the data set by discarding the examples which are less likely to add any new information for end task. As the core-set we obtain are aware of the downstream task, we called our approach as *Task-Aware Coreset (TA-Coreset)*. The number of examples that we select in a stage depends upon the budget size, \mathbf{b} . \mathbf{X}^s makes the selected examples set.

Oracle (C): We send the selected set, \mathbf{X}^s to the Oracle to query their labels. After retrieving their label, we append these examples along with their labels to

the set of labelled example ($\mathbf{X}^l = \mathbf{X}^l \cup \mathbf{X}^s$) and empty the selected set ($\mathbf{X}^s = \emptyset$). With this, we repeat another cycle till our budget limit.

Algorithm 1: k-Center-Greedy

Input: latent representation of data \mathbf{Z} , existing pool \mathbf{s}^0 and a budget b
Initialize $\mathbf{s} = \mathbf{s}^0$
repeat
 $u = \arg \max_{i \in [n] \setminus s} \min_{j \in s} \Delta(\mathbf{z}_i, \mathbf{z}_j)$
 $\mathbf{s} = \mathbf{s} \cup \{u\}$
until $|\mathbf{s}| = b + |\mathbf{s}^0|$
return $\mathbf{s} \setminus \mathbf{s}^0$

3 Experiments

Implementation Details: We trained pix2pix GAN as our task model for both depth estimation and polyps segmentation. We used Adam optimizer ($\beta_1 = 0.5, \beta_2 = 0.999$) with a learning rate of 2×10^{-4} for both generator and discriminator and used 200 as L_1 loss weight as in [12]. We trained the model for 100 epochs in each cycle with batch size of 20 for depth estimation and batch size of 8 for polyps segmentation. Unlike in [12], we used Instance Normalisation at each convolutional layer of both discriminator and generator.

For AL experimentation, we initialized our labelled pool with randomly selected 1310 examples for depth estimation, while keeping the sampling budget size of 655. In case of polyps segmentation, we initialized with randomly selected 100 examples keeping the same sampling budget size for following acquisition stages.

Data sets: We performed experiments on Colonoscopy Depth [12] and Kvasir-SEG [7]. Colonoscopy Depth is a synthetic data set consists of 16,380 images with their depth annotations. We divided the dataset into train, validation and test set in the ratio of 8:1:1, giving us 13104 training examples. Similarly, Kvasir-SEG consists of 1000 real images with polyp masks. We used 900 of them for training, and rest for validation. We reported our performance on a smaller test dataset provided by the same project consisting of 196 images.

Baselines: We have compared our method with a wide range of competitive baselines. **Random** is the most commonly used technique to sub-sample the training examples. We also applied Coreset [13] on low-dimensional feature representation computed in an unsupervised manner. We applied Principal Component Analysis (PCA) [16] and compressed the images to the dimension of 512 which is equal to that of the latent representations in our method. **Uncertainty** [8] is another sampling technique to find the most informative examples. Finally, we also compared our performance with **VAAL** [15] which is one of the current state-of-the-art task-agnostic active learning method.

Evaluation metrics: We report the performance of depth estimation in Root Mean Square Error (RMSE). Whilst, we evaluate the performance of semantic segmentation in mean Intersection Over Union (mIOU).

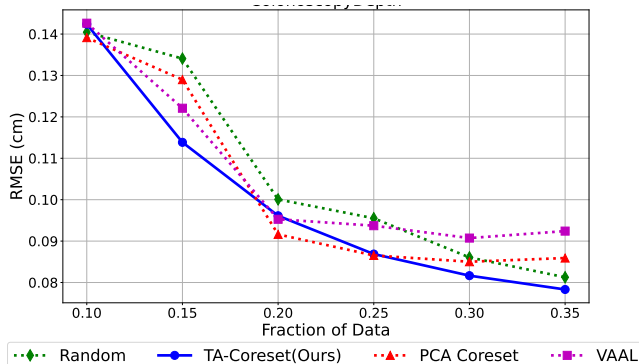


Fig. 3. Performance comparison on Colonoscopy Depth data set.

3.1 Depth Estimation:

Figure 3 shows the performance comparisons between the baselines and the proposed method. In the figure, the x-axis shows the fraction of total available data used to train the learner and the y-axis shows their corresponding RMSE reported in cm. From the graph, we can see that all the AL frameworks outperform the random sampling technique. Among the AL methods, the proposed method outperforms the others in most cases. PCA-coreset and VAAL are two task agnostic methods employing the sampling method on latent representations of the images. The performance of these two methods lags behind our pipeline. This gap in performance highlights the need of making the representations of the images task-aware. The performance of Random with 25% of examples is almost equivalent to the performance of TA-Coreset with 20% examples (or 30% with 25%). This is 20% reduction in the training examples.

3.2 Semantic Segmentation:

We also employed our method for polyp segmentation. Table 1 (upper block) summarises the performance comparison with the baselines. The first 100 examples in the experiments were randomly selected. In the table, we can observe that the performance of the random sampling is least compared to every AL methods. Among the AL methods, our TA-Coreset outperforms the rest in the every selection stages. Superior performance of our method compared to the task agnostic methods PCA-Coreset and VAAL validates our hypothesis. The performance of Random with 300 examples is almost equivalent to the performance of TA-Coreset with just 200 examples and so on.

Combining TA-Coreset with Uncertainty: In order to validate whether our method is complementary to another category of AL methods relying on uncertainties, we combine our method with that of Joshi et al. [8]. This is one of the most competitive baselines to select the informative examples and uses the difference of the best and the second best confidence score (BvSB) approach

Method	Mean IOU				
	100	200	300	400	500
Random	57.1	59.2	61.1	65.3	70.7
VAAL [15]	57.1	61.2	63.9	68.0	72.6
PCA-Coreset	57.1	58.2	62.2	66.8	70.2
TA-Coreset (ours)	57.1	61.8	66.9	71.2	74.5
Uncertainty + PCA [14]	57.1	60.0	63.0	65.8	72.6
Uncertainty + TA-Coreset	57.1	62.8	67.1	71.5	76.1

Table 1. Performance Comparison on Kvasir-SEG Dataset.

[8]. Less the difference in class prediction, more uncertain the model is about the example. We first sample N_u uncertain examples using uncertainty score given by BvSB. Then, we sample N_d diverse examples using TA-Coreset. The numbers N_u and N_d are controlled by a parameter γ such that $N_u = \gamma * N$ and $N_d = (1 - \gamma) * N$, where N is the total number of examples at a selection stage. Tab. 1 (lower block) shows the performance comparison with [14]. From the table, we can see that our method is complementary to existing methods based on uncertainties and also outperforms one of the state-of-the-art methods.

4 Qualitative Evaluations

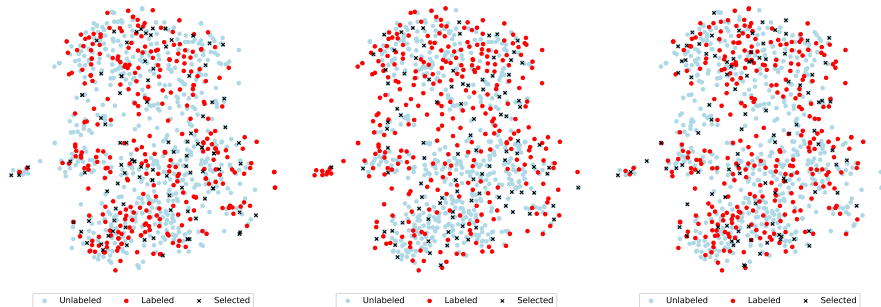


Fig. 4. T-SNE plots showing the comparison of selection of unlabelled examples at the fourth selection stage on Kvasir-SEG. Left, middle, and right plots show selection by Random, PCA-Coreset, and TA-Coreset, respectively (Zoom in for the better view).

In the Figure 4, we summarize the selection behaviour of different sampling techniques in Kvasir-SEG data set with help of the tSNE [10] plots. In the diagram, the grey dots are unlabelled examples, red dots labelled examples in previous selection stage, and the cross represents the examples selected in the current-stage for annotation. From these plots, random (left) selects the examples uniformly throughout the manifold. Similarly, PCA-coreset (middle) also

covers the whole manifold. While, TA-Coreset (right) covers manifold as a whole and also concentrate on some of the regions middle of the image manifold. These depict that sampling in task-aware latent representation is more important than selecting diverse examples on the task-agnostic image feature space.

5 Conclusions

In this paper, we present a novel task-aware active learning framework for endoscopic image analysis. We employed the proposed method on polyp segmentation and depth estimation. We observe a superior performance from the extensive experiments compared to the multiple competitive baselines, validating the proposed idea. Moreover, the generalisation of our method on two different tasks make it a generic method and exhibits a high potential to be equally effective in other tasks. We combined our method with the existing AL method and observed their performance improvement. And it demonstrates a complementary nature of our method.

6 Acknowledgement

This project is funded by the EndoMapper project by Horizon 2020 FET (GA 863146). For the purpose of open access, the author has applied a CC BY public copyright licence to any author accepted manuscript version arising from this submission.

References

1. Ahmad, O.F., Mori, Y., Misawa, M., Kudo, S.e., Anderson, J.T., Bernal, J., Berzin, T.M., Bisschops, R., Byrne, M.F., Chen, P.J., et al.: Establishing key research questions for the implementation of artificial intelligence in colonoscopy: a modified delphi method. *Endoscopy* **53**(09), 893–901 (2021)
2. Ali, S., Dmitrieva, M., Ghatwary, N., Bano, S., Polat, G., Temizel, A., Krenzer, A., Hekalo, A., Guo, Y.B., Matuszewski, B., et al.: Deep learning for detection and segmentation of artefact and disease instances in gastrointestinal endoscopy. *Medical image analysis* **70**, 102002 (2021)
3. Brandao, P., Mazomenos, E., Ciuti, G., Caliò, R., Bianchi, F., Menciassi, A., Dario, P., Koulaouzidis, A., Arezzo, A., Stoyanov, D.: Fully convolutional neural networks for polyp segmentation in colonoscopy. In: *Medical Imaging 2017: Computer-Aided Diagnosis*. vol. 10134, pp. 101–107. SPIE (2017)
4. Budd, S., Robinson, E.C., Kainz, B.: A survey on active learning and human-in-the-loop deep learning for medical image analysis. *Medical Image Analysis* **71**, 102062 (2021)
5. Caramalau, R., Bhattarai, B., Kim, T.K.: Sequential graph convolutional network for active learning. In: *Proceedings of the IEEE/CVF Conference on Computer Vision and Pattern Recognition*. pp. 9583–9592 (2021)

6. Cardoso, J., Van Nguyen, H., Heller, N., Abreu, P.H., Isgum, I., Silva, W., Cruz, R., Amorim, J.P., Patel, V., Roysam, B., et al.: Interpretable and Annotation-Efficient Learning for Medical Image Computing: Third International Workshop, iMIMIC 2020, Second International Workshop, MIL3ID 2020, and 5th International Workshop, LABELS 2020, Held in Conjunction with MICCAI 2020, Lima, Peru, October 4–8, 2020, Proceedings, vol. 12446. Springer Nature (2020)
7. Jha, D., Smedsrud, P.H., Riegler, M.A., Halvorsen, P., Lange, T.d., Johansen, D., Johansen, H.D.: Kvasir-seg: A segmented polyp dataset. In: International Conference on Multimedia Modeling. pp. 451–462. Springer (2020)
8. Joshi, A.J., Porikli, F., Papanikolopoulos, N.: Multi-class active learning for image classification. In: 2009 IEEE conference on computer vision and pattern recognition. pp. 2372–2379. IEEE (2009)
9. Li, C.T., Tsai, H.W., Yang, T.L., Lin, J.C., Chow, N.H., Hu, Y.H., Cheng, K.S., Chung, P.C.: Imbalance-effective active learning in nucleus, lymphocyte and plasma cell detection. In: Interpretable and Annotation-Efficient Learning for Medical Image Computing, pp. 223–232. Springer (2020)
10. Van der Maaten, L., Hinton, G.: Visualizing data using t-sne. *Journal of machine learning research* **9**(11) (2008)
11. Mahapatra, D., Bozorgtabar, B., Thiran, J.P., Reyes, M.: Efficient active learning for image classification and segmentation using a sample selection and conditional generative adversarial network. In: International Conference on Medical Image Computing and Computer-Assisted Intervention. pp. 580–588. Springer (2018)
12. Rau, A., Edwards, P., Ahmad, O.F., Riordan, P., Janatka, M., Lovat, L.B., Stoyanov, D.: Implicit domain adaptation with conditional generative adversarial networks for depth prediction in endoscopy. *International journal of computer assisted radiology and surgery* **14**(7), 1167–1176 (2019)
13. Sener, O., Savarese, S.: Active learning for convolutional neural networks: A core-set approach. In: International Conference on Learning Representations (2018)
14. Shi, X., Dou, Q., Xue, C., Qin, J., Chen, H., Heng, P.A.: An active learning approach for reducing annotation cost in skin lesion analysis. In: International Workshop on Machine Learning in Medical Imaging. pp. 628–636. Springer (2019)
15. Sinha, S., Ebrahimi, S., Darrell, T.: Variational adversarial active learning. In: Proceedings of the IEEE/CVF International Conference on Computer Vision. pp. 5972–5981 (2019)
16. Wold, S., Esbensen, K., Geladi, P.: Principal component analysis. *Chemometrics and intelligent laboratory systems* **2**(1-3), 37–52 (1987)
17. Yang, L., Zhang, Y., Chen, J., Zhang, S., Chen, D.Z.: Suggestive annotation: A deep active learning framework for biomedical image segmentation. In: International conference on medical image computing and computer-assisted intervention. pp. 399–407. Springer (2017)
18. Zhu, J.Y., Park, T., Isola, P., Efros, A.A.: Unpaired image-to-image translation using cycle-consistent adversarial networks. In: ICCV (2017)

7 Appendix

Figure 5 and 6 show the qualitative comparison of the models trained on data annotated at the *third* selection stage. From these comparisons, we can observe that the proposed method is able to select the examples from the manifolds where the model is uncertain, whereas the baselines fail (1 B).

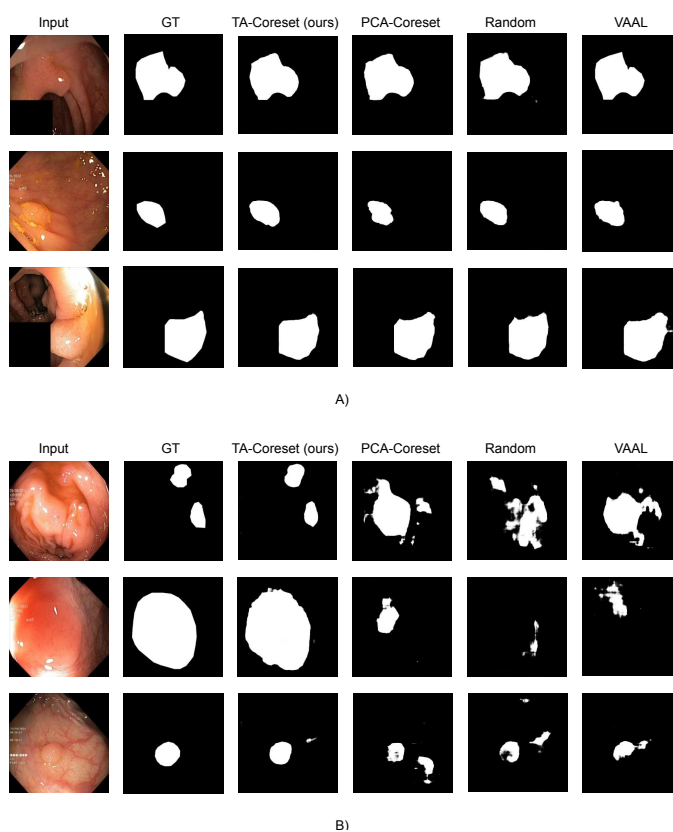


Fig. 5. Qualitative comparisons on Kvasir-SEG Dataset[7]: A) Examples with Similar Performance B) Examples where our method performs best

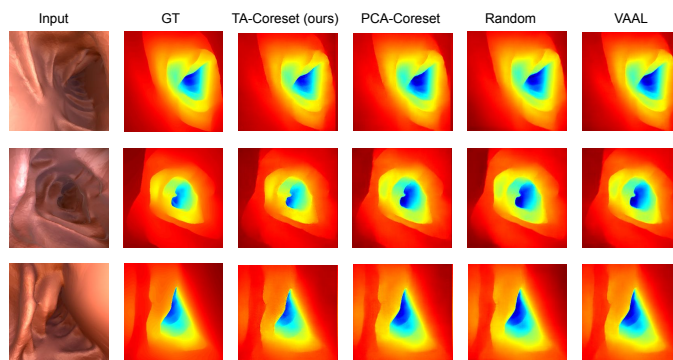


Fig. 6. Qualitative comparisons on Colonoscopy Depth Dataset

8 Combining Uncertainty and TA-Coreset: Ablation

We performed experiments on combining samples from Uncertainty based acquisition function and TA-Coreset. We experimented with different values of γ , which corresponds to fraction of uncertain examples to sample from total budget. The test results on Kvasir-SEG [7] is shown in figure 7. We found out that equally balancing uncertainty and diversity ($\gamma = 0.5$) while sampling performed best. The setting closer to TA-Coreset ($\gamma = 0.1$) showed similar trend to TA-Coreset itself. We see similar trend to its counterpart in case of heavy uncertainty sampling ($\gamma = 0.75$) as well.

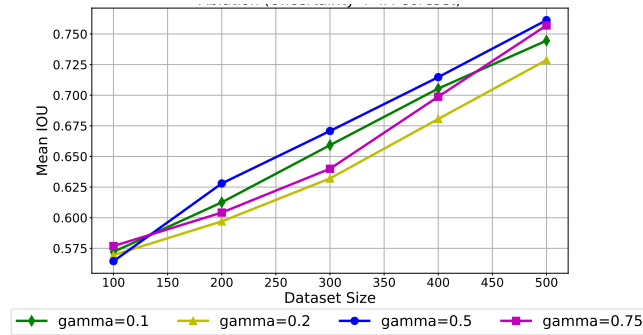


Fig. 7. Ablation study on different combinations of Uncertainty and TA-Coreset